THE JOURNAL OF BIOLOGICAL CHEMISTRY VOL. 288, NO. 29, pp. 20883–20895, July 19, 2013

α-Synuclein Senses Lipid Packing Defects and Induces Lateral Expansion of Lipids Leading to Membrane Remodeling*

Received for publication, April 17, 2013, and in revised form, June 5, 2013 Published, JBC Papers in Press, June 5, 2013, DOI 10.1074/jbc.M113.478297

Myriam M. Ouberai[‡1], Juan Wang[§], Marcus J. Swann[§], Celine Galvagnion[¶], Tim Guilliams[¶], Christopher M. Dobson[¶], and Mark E. Welland[‡]

From the [‡]Nanoscience Centre, Department of Engineering, University of Cambridge, Cambridge CB3 0FF, United Kingdom, the [§]Farfield Group Ltd., Biolin Scientific, Voyager, Chicago Avenue, Manchester M90 3DQ, United Kingdom, and the [¶]Department of Chemistry, University of Cambridge, Lensfield Road, Cambridge CB2 1EW, United Kingdom

Background: α-Synuclein folds into an amphipathic α-helical structure upon membrane interaction.
Results: The binding is promoted by lipid packing defects found in vesicles of high curvature and in planar membranes with cone-shaped lipids.
Conclusion: The insertion of α-synuclein induces a lateral expansion of lipids that can progress to membrane remodeling.
Significance: These findings support the role of α-synuclein in vesicle trafficking.

There is increasing evidence for the involvement of lipid membranes in both the functional and pathological properties of α-synuclein (α-Syn). Despite many investigations to characterize the binding of α-Syn to membranes, there is still a lack of understanding of the binding mode linking the properties of lipid membranes to α-Syn insertion into these dynamic structures. Using a combination of an optical biosensing technique and *in situ* atomic force microscopy, we show that the binding strength of α-Syn is related to the specificity of the lipid environment (the lipid chemistry and steric properties within a bilayer structure) and to the ability of the membranes to accommodate and remodel upon the interaction of α-Syn with lipid membranes. We show that this interaction results in the insertion of α-Syn into the region of the headgroups, inducing a lateral expansion of lipid molecules that can progress to further bilayer remodeling, such as membrane thinning and expansion of lipids out of the membrane plane. We provide new insights into the affinity of α-Syn for lipid packing defects found in vesicles of high curvature and in planar membranes with cone-shaped lipids and suggest a comprehensive model of the interaction between α-Syn and lipid bilayers. The ability of α-Syn to sense lipid packing defects and to remodel membrane structure supports its proposed role in vesicle trafficking.

α-Synuclein (α-Syn)[2] is a 140-amino acid residue presynaptic protein whose aggregation is related to the neurodegenerative disorder Parkinson disease (1). This protein is abundant in the central nervous system, and it is found as a cross-β-sheet-rich structure within protein deposits in both sporadic and dominant familial forms of the disease (2). Although the biological function of α-Syn remains unclear, various studies suggest that it plays roles in modulating synaptic plasticity, presynaptic vesicle pool size, and neurotransmitter release (3). There is considerable evidence to suggest that α-Syn associates with synaptic vesicles, both *in vivo* and *in vitro* (4, 5). Indeed, membrane binding has been suggested to inhibit vesicle docking and fusion as well as being the cause of vesicle clustering because of the tendency of α-Syn to aggregate and ultimately contribute to its pathobiology (6).

α-Syn is composed of a highly conserved sequence (KTKEGV) repeated imperfectly throughout the N-terminal half of the protein that can be displayed as an amphipathic helix upon binding to membranes (7). In this conformation, these repeats generate an unbalanced distribution of polar and nonpolar residues that form separate hydrophobic and polar faces, a distribution well fitted for membrane binding (8–10). This arrangement is similar to amphipathic lipid-packing sensor motifs (ALPS motifs) that sense membrane curvature and are found in various proteins, such as ArfGAP1, a Golgi-associated protein, and antimicrobial peptides, including melittin (7, 11). These motifs are known to use bulky hydrophobic residues to sense the defects in lipid packing due to a mismatch between the curvature of the bilayer and the shape of the lipids (12). Although α-Syn and ALPS motifs have distinct sequences, they both have the ability to sense membrane curvature (13).

A large number of studies have been carried out to probe the interaction of α-Syn with lipid membranes using membrane mimics, such as large and small unilamellar vesicles (LUVs and SUVs, respectively) and supported lipid bilayers (SLBs). Membrane curvature as well as lipid composition have been reported to have a high impact on α-Syn binding (14–16). α-Syn interacts with phospholipid membranes and particularly with acidic phospholipids, a phenomenon attributed to the electrostatic attractions with the lysine residues found in the N-terminal region of the protein (17). Furthermore, α-Syn has been reported to associate with lipid rafts, lipid domains enriched in cholesterol and sphingomyelin, as well as with gangliosides (18,

* This work was supported by Biotechnology and Biological Sciences Research Council Grant BB/H003843/1, European Union (EU) training network project NEURASYNC, EU FP6 project ASMENA, Élan plc, and Parkinson's UK Grant H-0903.

[1] To whom correspondence should be addressed. Tel.: 44-01223-760303; Fax: 44-1223-760309; E-mail: mmo25@cam.ac.uk.

[2] The abbreviations used are: α-Syn, α-synuclein: ALPS, amphipathic lipid-packing sensor motifs; LUV, large unilamellar vesicle; SUV, small unilamellar vesicle; SLB, supported lipid bilayer; AFM, atomic force microscopy; DPI, dual polarization interferometry; DOPC, 1,2-dioleoyl-*sn*-glycero-3-phosphocholine; DOPE, 1,2-dioleoyl-*sn*-glycero-3-phosphoethanolamine; DOPS, 1,2-dioleoyl-*sn*-glycero-3-phospho-L-serine; BTLE, brain total lipid extract; PE, phosphatidylethanolamine.

19). It has been shown that α-Syn binds small (20–25-nm) unilamellar vesicles in preference to larger (125-nm) vesicles of a given composition (17). This effect has been attributed to the fact that the initial insertion process is facilitated by the existence of lipid packing defects caused by membrane curvature (16). However, no clear correlation has yet been proposed between the membrane curvature and the mode of binding. The structure of membrane-bound α-Syn determined in the presence of micelles or small unilamellar vesicles shows that α-Syn adopts an extended and/or broken curved α-helical conformation that extends parallel to the membrane surface (8, 20, 21).

Despite the fact that many studies have characterized the interaction of α-Syn with lipid membranes, there are still major questions remaining to be answered in the context of the effect of protein binding on membrane structure and how this process is linked to the mechanism of interaction. The binding of α-Syn to membranes might induce the permeabilization of lipid bilayers via pore or conductive ion channel formation (22–25). Alternatively, α-Syn has been suggested to induce membrane remodeling events, such as the nascent budding and tubulation of vesicles (26–28). In terms of the impact of such an interaction on aggregation, it has been reported that lipid binding inhibits fibril formation (18, 29) or promotes the formation of aggregates at the membrane surface (30–33). These diverse and often contradictory effects induced by α-Syn on membranes arise from a lack of clarity of the binding mode as well as the use of lipid compositions that are sometimes far removed from those relevant to physiological conditions, such as highly negatively charged lipid bilayers.

In this report, we describe the use of a combination of an optical biosensing technique, dual polarization interferometry (DPI), and *in situ* atomic force microscopy (AFM) studies to propose a model of interaction and explain the impact on the binding of membrane environment properties in terms of lipid composition (the lipid chemistry and steric properties) and bilayer structure. DPI is a unique technique that makes real-time thickness and refractive index measurements of thin isotropic layers deposited on the top of a sensing waveguide (34, 35). In the case of an anisotropic layer, such as a lipid bilayer, the mass and the birefringence can be monitored, providing highly valuable information about the mode of interaction of proteins with lipid membranes by monitoring the changes in lipid ordering (36–39). The binding mode was studied here using mixtures of common phospholipids found in membranes and with a physiologically relevant lipid composition. Importantly, comparisons are also made between small and large vesicles and planar supported lipid bilayers. The results reveal that, as well as an enhancement of binding due to electrostatic interaction, the binding of α-Syn to lipid bilayers is modulated by the presence of lipid packing defects, such as the presence of cone-shaped lipids and curved lipid bilayers, and that the formation of pores is unlikely to occur. Interestingly, we show that the binding affinity to lipid bilayers containing cone-shaped lipids is significantly enhanced, causing the observed trend with bilayer curvature to be the opposite of the curvature sensing model. On the basis of all of our results, we propose a comprehensive model of the interaction of α-Syn with lipid membranes. This interaction is promoted by lipid packing defects as the insertion of α-Syn into lipid bilayers induces a lateral expansion of lipids and can further progress toward membrane remodeling processes, such as membrane thinning and expansion of lipid molecules out of the membrane plane.

EXPERIMENTAL PROCEDURES

Materials—Expression and purification of WT α-synuclein was carried out according to a published protocol with minor modifications (40). Melittin was purchased from Calbiochem. Lipids, Avanti miniextruder, and polycarbonate filters were obtained from Avanti Polar Lipids. Sodium dodecyl sulfate (SDS) was purchased from Sigma. Tris-buffered saline (TBS) solution, pH 7.4 (25 mM Tris, 137 mM NaCl, 2.7 mM KCl) was obtained from Fisher, and *N*-hydroxysuccinimidyl-PEG_4-Biotin was from Thermo. The memLAYER lipid vesicle coupling kit was obtained from Layerlab AB and comprised NeutrAvidin™ and single strand DNA oligomers with biotin or cholesterol termination: Biotin-ssDNA, cholesterol-ssDNA 1S, and cholesterol-ssDNA 1L.

Vesicle Preparation—Vesicles composed of 1,2-dioleoyl-*sn*-glycero-3-phosphocholine (DOPC)/1,2-dioleoyl-*sn*-glycero-3-phosphoethanolamine (DOPE)/1,2-dioleoyl-*sn*-glycero-3-phospho-L-serine (DOPS) (in a 20:50:30 mass ratio), DOPC/DOPE/DOPS (in a 50:20:30 mass ratio), DOPC/DOPS (in a 70:30 mass ratio), DOPC, and brain total lipid extract (BTLE) were prepared by extrusion in the case of LUVs and sonication for SUVs. BTLE is a chloroform/methanol extract of brain tissue that contains common phospholipids found in membranes and other components, such as lipoproteins, cholesterol, cerebrosides, ceramides, and sphingolipids. However, no extensive analytical data are available for this natural extract. The required amounts of lipid were dissolved in $CHCl_3/CH_3OH$ (2:1, v/v) and mixed in the appropriate ratios. The solvent was removed by using a stream of N_2 gas. Dried films were maintained under reduced pressure overnight and thereafter hydrated in TBS, pH 7.4. The hydration led to the formation of large multilamellar vesicles with a lipid concentration of 4–5 mg/ml. LUVs were generated by three cycles of freeze/thawing and 21 cycles of extrusion through a polycarbonate filter of 100 nm using the Avanti miniextruder. Sonication of large multilamellar vesicle suspensions typically produces SUVs with diameters in the range of 15–50 nm. A bath sonicator (Aries 101, Farfield) with a frequency of 37 kHz and an effective ultrasonic power of 35 watts (waveform peak power of 280 watts) was used. Glass vials with large multilamellar vesicle dispersion were suspended in the bath sonicator and sonicated for 10 min with 5-min intervals for at least six cycles or until the solution became transparent. The size and polydispersity of vesicle suspensions were monitored by dynamic light scattering with a Zetasizer Nano ZS (Malvern Instruments).

Dual Polarization Interferometry—An *Ana*light 4D dual polarization interferometer containing a silicon oxynitride FB80 AnaChip was used to perform all dual polarization interferometry measurements (Farfield Group, Biolin Scientific AB). The technique uses a dual slab optical waveguide sensor into which light polarized in one of two orthogonal directions is alternately coupled. The polarized light excites either transverse electric or transverse magnetic modes in the two waveguides. Light travels along the upper sensing and lower refer-

ence waveguides, emerging to form an interference pattern, which is measured by the instrument. Each mode generates an evanescent field above the top sensing waveguide surface, which is exposed to the sample solution. This field interacts with material coming into contact with the sensor surface and results in a change in the propagation of the light in each mode and hence the measured signal. The measured phase change data from the two polarization modes are analyzed with the *Ana*light DPI Explorer software which uses Maxwell's equations for the distribution of light in a waveguide to determine the refractive index and thickness of an equivalent uniform isotropic layer on top of the sensing waveguide surface. The mass per unit area of an adsorbed layer can be determined from thickness and refractive index using the Feijter formula, which uses the refractive index increments (d*n*/d*c*) of the lipid and protein, which are 0.135 and 0.182 ml/g, respectively, as reported previously (36, 41). Alternatively, where the layer on the surface of the waveguide is birefringent, as is the case for SLBs, the refractive index (or thickness) of the layer can be assumed to be constant, and the thickness (or refractive index) and birefringence can be calculated (36, 37). The birefringence or optical anisotropy measures the difference in refractive index of the two orthogonal polarizations caused by the net alignment of the lipid molecules perpendicular to the waveguide surface that creates an anisotropic system. In this case, the measured birefringence provides information about the level of order or alignment in the plane perpendicular to the bilayer surface, whereas the mass is simply proportional to the thickness measured. Changes in the thickness and hence mass of the layer were determined by assuming a fixed refractive index of 1.47 for the bilayer. The deposition of the bilayers was monitored by the rate of change in mass and by the evolution of birefringence. The change in birefringence as a function of the mass of protein bound, which relates to an average change of lipid molecular orientation order, was then used to characterize the effect of protein binding on membrane structure and bilayer order. Protein/lipid mass ratio values were calculated using the mass values of the corresponding SLBs prior to protein injection, together with the additional mass gain after protein injection. The mass changes were determined using the d*n*/d*c* values for proteins and lipids of 0.182 and 0.135 ml/g, respectively (36).

Preparation of Supported Lipid Bilayers—An independent Harvard Apparatus PHD2000 programmable syringe pump was used to control the flow rate of the bulk running buffer. The instrument was set to operate at 25.0 ± 0.1 °C, and the bulk buffer used was TBS, pH 7.4, for lipid bilayer formation and for protein-lipid binding experiments. The chip was cleaned using a UV-ozone procedure and allowed to stabilize prior to the experiment. The optical properties of the chip were then calibrated at 25 °C using 80% (w/w) ethanol and water, followed by calibration of the bulk buffers. The final vesicle solution was then infused at 15 μl/min, forming a stable bilayer in the presence of 5 mM $CaCl_2$. The bilayer was then left to equilibrate for 30 min. When the signal from the chip had stabilized, protein or peptide solution was infused at 25 μl/min for 5 min in order to observe binding events followed by TBS for at least 10 min. α-Syn and melittin were dissolved in bulk buffer and injected at the desired concentration onto each membrane in successive experiments, the surface being cleaned with 2% SDS and ethanol and a new bilayer formed between experiments.

Preparation of Tethered Vesicle Surfaces—The immobilization of vesicles on chip surfaces was carried out according to a published protocol with some slight modifications (42). Silicon oxynitride waveguides prefunctionalized with amine groups were used (Farfield Group, Biolin Scientific AB). *N*-Hydroxysuccinimidyl-PEG_4-biotin was dissolved in PBS, and about 150 μl of the solution was dropped onto the amine chip surface and then left to stand for 30 min at room temperature. Excess solution was washed from the surface with water and ethanol. The chip was dried by using a stream of N_2 gas and used directly or stored in the freezer for future experiments. The vesicles were tethered to the surface via the hybridization of complementary DNA strands. On the previously prepared biotinylated surfaces, 1:1 mixtures of NeutrAvidin (10 μg/ml) and biotin-ssDNA (170 nM; biotin at the 3′-end of ssDNA) were infused at a flow rate of 25 μl/min, resulting in a ssDNA surface that can hybridize with the complementary DNA tags on the vesicles. The cholesterol-dsDNA tag was first obtained by hybridization of the two cholesterol-labeled ssDNAs at 1.3 μM, one long strand and one short strand, with the overlapping part complementary in sequence. The cholesterol moieties are covalently bound to the double-stranded end, one at each strand. The single-stranded end of the cholesterol-DNA tag is complementary in sequence to the biotin-ssDNA on the chip surface. The cholesterol-ds-DNA tags were mixed with vesicles to give 85 nM DNA and 1 mg/ml lipid and left for at least 40 min. The cholesterol moieties then penetrate into the lipid membrane so as to anchor the DNA tags to the surface of the vesicles. The cholesterol-ds-DNA-tagged vesicles were introduced to the biotin-ssDNA surface at a low flow rate and incubated for about 40 min so that the DNA hybridized and vesicles became anchored. After the introduction of the vesicles, the surface was rinsed in the running buffer before injection of protein or peptide solutions. The molecular transport of sucrose across vesicle membranes due to lipid bilayer permeabilization was examined by monitoring the variation in the phase changes during injections of 0.1 M sucrose in TBS as described previously (42).

Circular Dichroism (CD) Spectroscopy—Far-UV CD spectra of α-Syn were acquired in TBS at 25 °C. α-Syn was diluted to a final concentration of 10 μM, and the spectra were acquired using a 1-mm path length cuvette and a J-810 Jasco spectropolarimeter (Tokyo, Japan), equipped with a thermostated cell holder. Spectra were obtained by averaging five scans recorded in the 200–250-nm wavelength range using a scan rate of 50 nm/min, bandwidth of 1 nm, and 4-s time response.

Atomic Force Microscopy—A PicoPlus AFM with a PicoSPMII controller from Molecular Imaging was used for the imaging study. Images were acquired in solution at room temperature using the Mac Mode with Type I MAC Levers (Agilent) with the force constant varying from 0.6 to 1.75 newtons/m. Lipid vesicles were incubated in TBS, pH 7.4, with 5 mM $CaCl_2$ in a liquid cell over a freshly cleaved mica surface for between 30 and 60 min. The supported lipid bilayer formed on the mica was then thoroughly rinsed with TBS, pH 7.4, and the structure of the lipid bilayer was imaged before incubation with protein. Follow-

TABLE 1

Structural parameters of phospholipid membrane environments

The values are the mean of three determinations ± S.D. The SLB thickness and birefringence values were calculated from the transverse magnetic and transverse electric phase changes using the assumed isotropic refractive index (*n*) of 1.47. The LUV and SUV refractive index and thickness values were calculated assuming a uniform isotropic layer model. The mass values of both layers were calculated from the thickness and RI using the d*n*/d*c* value for lipids of 0.135 ml/g. For the vesicles, the thickness and refractive index values were calculated as an additional layer on top of the underlying NeutrAvidin layer.

Lipid bilayer structure	Lipid composition	RI	Thickness	Mass	Birefringence
			nm	*ng/mm²*	
SLB	DOPC/DOPE/DOPS (20:50:30)	1.47	5.2 ± 0.3	5.2 ± 0.3	0.0191 ± 0.0007
	DOPC/DOPE/DOPS (50:20:30)	1.47	4.6 ± 0.2	4.6 ± 0.2	0.0172 ± 0.0004
	DOPC/DOPS (70:30)	1.47	4.50 ± 0.04	4.52 ± 0.04	0.0158 ± 0.0002
	DOPC	1.47	4.6 ± 0.3	4.6 ± 0.3	0.017 ± 0.001
LUV	DOPC/DOPE/DOPS (20:50:30)	1.349 ± 0.003	107 ± 38	10.4 ± 2.1	
	DOPC/DOPS (70:30)	1.3554 ± 0.0001	52 ± 5	7.9 ± 0.6	
	DOPC	1.356 ± 0.001	56 ± 12	8.6 ± 0.9	
SUV	DOPC/DOPE/DOPS (20:50:30)	1.354 ± 0.004	39 ± 9	5.4 ± 0.4	
	DOPC/DOPS (70:30)	1.362 ± 0.003	19 ± 2	3.80 ± 0.06	
	DOPC	1.356 ± 0.001	28 ± 6	4.4 ± 0.7	

ing the introduction of protein, imaging was again carried out, and the effects on the structure of the lipid bilayers were recorded in the same area over the course of 60 min. The images presented are representative of the processes occurring in the samples because a range of different areas among several sets of experiments have been examined to verify reproducibility.

RESULTS

Characterization of Phospholipid Membrane Environments

Supported Lipid Bilayers—Prior to protein binding, phospholipid membranes were formed on a DPI chip surface and characterized in terms of mass (via thickness) and birefringence. Supported lipid bilayers were formed by adsorption and rupture of large unilamellar vesicles of the corresponding lipid mixture on the silicon oxynitride surface. Stable planar bilayers were obtained after rinsing with buffer and water to remove unruptured vesicles. The thickness and birefringence values vary according to the lipid compositions, as shown in Table 1. The DOPC SLB was found to be 4.6 ± 0.3 nm in thickness, corresponding to a surface area per lipid molecule of 0.53 nm^2. These data correlate well with expected values of the phosphatidylcholine headgroup, which requires a molecular area of 0.47–0.54 nm^2 (43) and with literature mass values (36). Adding DOPS gives rise to the same mass coverage and a birefringence with a similar or slightly lower value. The presence of a small amount of DOPE leads to a similar mass deposition and an increase in birefringence from 0.0158 ± 0.0002 to 0.0172 ± 0.0004. This trend is confirmed with the mixture containing 50% (w/w) DOPE, for which the birefringence shows the highest value observed in this study, 0.0191 ± 0.0007, which can be related to a higher level of order of the SLB. This effect is associated with the highest mass deposited, which corresponds to the lowest surface area per lipid. This observation is in good agreement with the lower molecular surface area required for PE phospholipids compared with phosphatidylcholine phospholipids (43).

Tethered Vesicles—Vesicles were tethered to the surface of the chip by the hybridization of a cholesterol-modified DNA molecule incorporated into the vesicles and a complementary DNA-biotin previously immobilized to a NeutrAvidin layer on the surface (42). The large unilamellar vesicles composed of DOPC/DOPE/DOPS (20:50:30) formed a layer of 107 ± 38 nm in thickness, which matches well with the range of the diameter values of LUV measured using dynamic light scattering (106 nm, diameter with the highest frequency in number size distribution for one set of experiments). SUVs composed of the same mixture formed a layer with a value of 39 ± 9 nm in thickness that also corresponds to the range of the diameter values of vesicles measured by dynamic light scattering (33 nm, diameter with the highest frequency in number size distribution for one set of experiments). For the DOPC/DOPS (70:30) and DOPC LUVs, the thickness values measured by DPI were lower than expected and probably not attributable solely to differences in vesicle size. These reduced thickness values could be related to a degree of vesicle distortion and/or to a lower coverage, which would lead to the underestimation of the thickness. Some distortion of vesicles upon tethering has been reported previously (44). However, irrespective of this effect, neither the relative mass calculation, to provide protein/lipid ratios, nor the sequence of relative curvatures between the different sizes of vesicles would be affected. Therefore, this observation has no impact on the findings presented here.

α-Syn Binding to SLBs of Different Compositions

In order to investigate the effect of lipid composition on α-Syn binding, the variations in mass and birefringence were monitored upon protein incubation with, and during rinsing from, the SLBs (Fig. 1). At the maximum binding observed during the incubation time, mass and birefringence values were extracted, and the resulting mass and molar ratios as well as the degree of disruption of the bilayer order (percentage of birefringence change compared with the initial value) were calculated (Table 2). α-Syn showed a relatively low binding affinity to DOPC SLB with a protein/lipid mass ratio value of 0.0011 ± 0.0004 and showed only a slight increase in birefringence, indicating the absence of bilayer disruption (Table 2). The presence of DOPS induced significantly higher binding of α-Syn, with a protein/lipid mass ratio value of 0.025 ± 0.002, an observation that can be attributed to electrostatic interactions between the negatively charged headgroups of DOPS and the positively charged residues of the protein. Interestingly, increasing the content of DOPE in SLBs, while keeping the same amount of DOPS, induced a much higher binding of α-Syn, with a protein/lipid mass ratio value of 0.05 ± 0.02 for DOPC/DOPE/DOPS (50:20:30) and 0.14 ± 0.02 for DOPC/DOPE/DOPS (20:50:30). This mass ratio for DOPC/DOPE/DOPS (20:50:30) corre-

sponds to a molar ratio of 137 ± 16 lipids/protein, a value that is significantly lower than the ratios observed without or with a low amount of DOPE.

To probe the conformational rearrangement of α-Syn upon interaction with lipid bilayers, a circular dicroism spectroscopy study was performed. As displayed in Fig. 2, a shift toward an α-helical conformation (characteristic minima around 208 and 222 nm) upon interaction with DOPC/DOPE/DOPS (20:50:30) LUVs was observed, in good agreement with previous works (10, 17).

The birefringence changes as a function of the protein/lipid mass ratio (Fig. 1*B*) show, except for DOPC, two processes for α-Syn binding to different SLBs. During the initial binding stage, there is a sharp decrease in birefringence (about 6% of the initial values) along with a relatively small increase in mass (or mass decrease in the case of DOPC/DOPE/DOPS (20:50:30), which will be discussed below). During the second stage, although there is a much greater increase in the protein/lipid mass ratios, indicating a higher level of binding of α-Syn, the birefringence remains almost unchanged. This indicates that α-Syn might partially penetrate into the SLB during the first binding stage; however, it appears that further binding of α-Syn does not lead to greater disruption (in the plane perpendicular to the bilayer surface) of the SLB structure. This observation suggests that α-Syn is binding onto the outer layer of the SLBs (*i.e.* in the region of the headgroups). After the protein binding event, a low mass desorption is observed during rinsing with buffer, which indicates a low degree of reversibility.

To support the relationship between the changes in birefringence and binding modes, the effects of a well known antimicrobial peptide melittin were studied on the DOPC/DOPE/DOPS (20:50:30) lipid mixture (Fig. 1). Upon melittin binding to the SLB, the mass increase is associated with a continuous

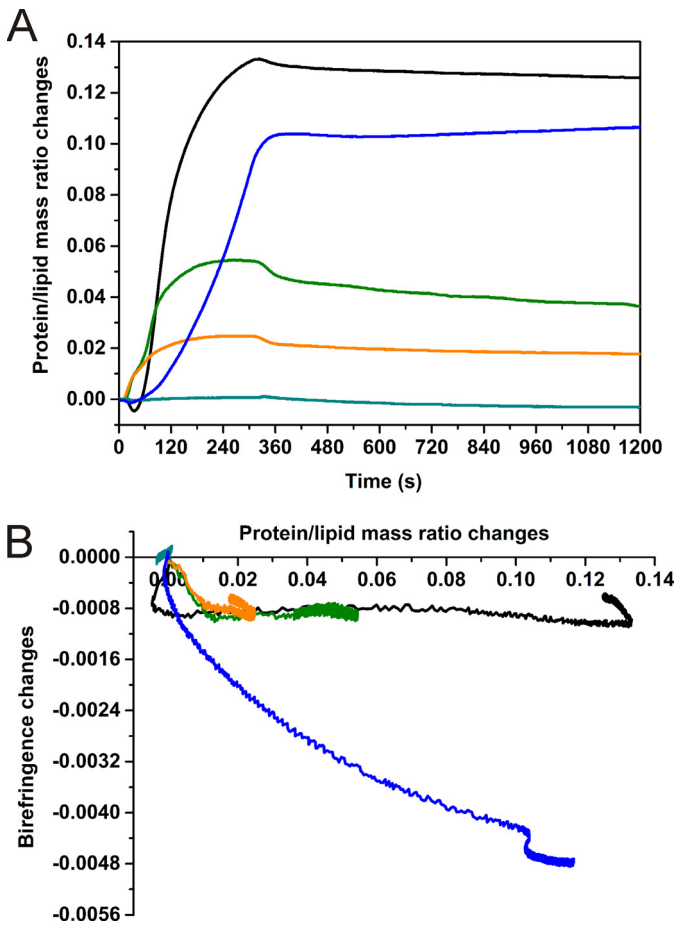

FIGURE 1. **Effect of α-Syn binding on SLBs of different compositions.** Plots of the protein/lipid mass ratio changes as a function of time (*A*) and of the birefringence changes as a function of the changes in protein/lipid mass ratio (*B*) in TBS, pH 7.4: α-Syn 2.5 μM binding to SLBs composed of DOPC/DOPE/DOPS (20:50:30) (*black line*), DOPC/DOPE/DOPS (50:20:30) (*green line*), DOPC/DOPS (70:30) (orange line), and DOPC (*cyan line*); melittin 2.5 μM binding to SLB composed of DOPC/DOPE/DOPS (20:50:30) (*blue line*). Protein injections were performed for 5 min, followed by rinsing time with TBS for at least 30 min. Protein/lipid mass ratio values were calculated using the mass values of the corresponding SLBs prior to protein injection together with the additional mass gain after protein injection. The mass changes were determined using the d*n*/dc values for proteins and lipids of 0.182 and 0.135 ml/g, respectively (36).

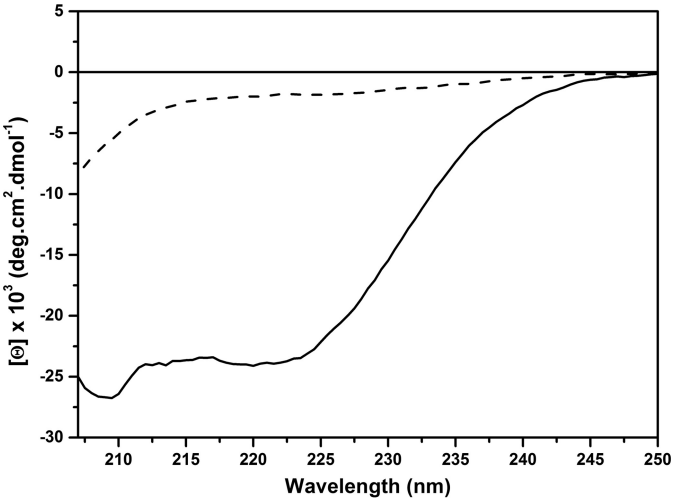

FIGURE 2. **Change in the secondary structure of α-Syn upon interaction with DOPC/DOPE/DOPS (20:50:30) LUVs examined by circular dichroism spectroscopy.** Shown is α-Syn at 10 μM in TBS (*dashed line*) and in the presence of 10 mM DOPC/DOPE/DOPS (20:50:30) LUVs in TBS (*solid line*).

TABLE 2

Experimental parameters of protein-supported lipid bilayer interactions

The values are the mean of three determinations ± S.D.

SLB	Protein	ΔMass	Protein/lipid mass ratio[a]	Lipid/protein molar ratio	ΔBirefringence	Disruption[b]
		ng/mm²				%
DOPC/DOPE/DOPS (20:50:30)	α-Syn	0.72 ± 0.09	0.14 ± 0.02	137 ± 16	−0.00118 ± 0.00009	−6 ± 1
	Melittin	0.9 ± 0.5	0.19 ± 0.09	115 ± 50	−0.0057 ± 0.0008	−30 ± 3
DOPC/DOPE/DOPS (50:20:30)	α-Syn	0.22 ± 0.08	0.05 ± 0.02	431 ± 162	−0.0011 ± 0.0003	−6 ± 2
DOPC/DOPS (70:30)	α-Syn	0.11 ± 0.01	0.025 ± 0.002	734 ± 76	−0.0009 ± 0.0001	−5 ± 1
DOPC	α-Syn	0.005 ± 0.002	0.0011 ± 0.0004	18746 ± 6709	0.00014 ± 0.00003	0.8 ± 0.1

[a] Protein/lipid mass ratio values were calculated using the mass values of the corresponding SLBs prior to protein injection, together with the additional mass gain after protein injection. The mass changes were determined using the d*n*/dc values for proteins and lipids of 0.182 and 0.135 ml/g, respectively (36).

[b] Percentage of birefringence change compared with the initial value.

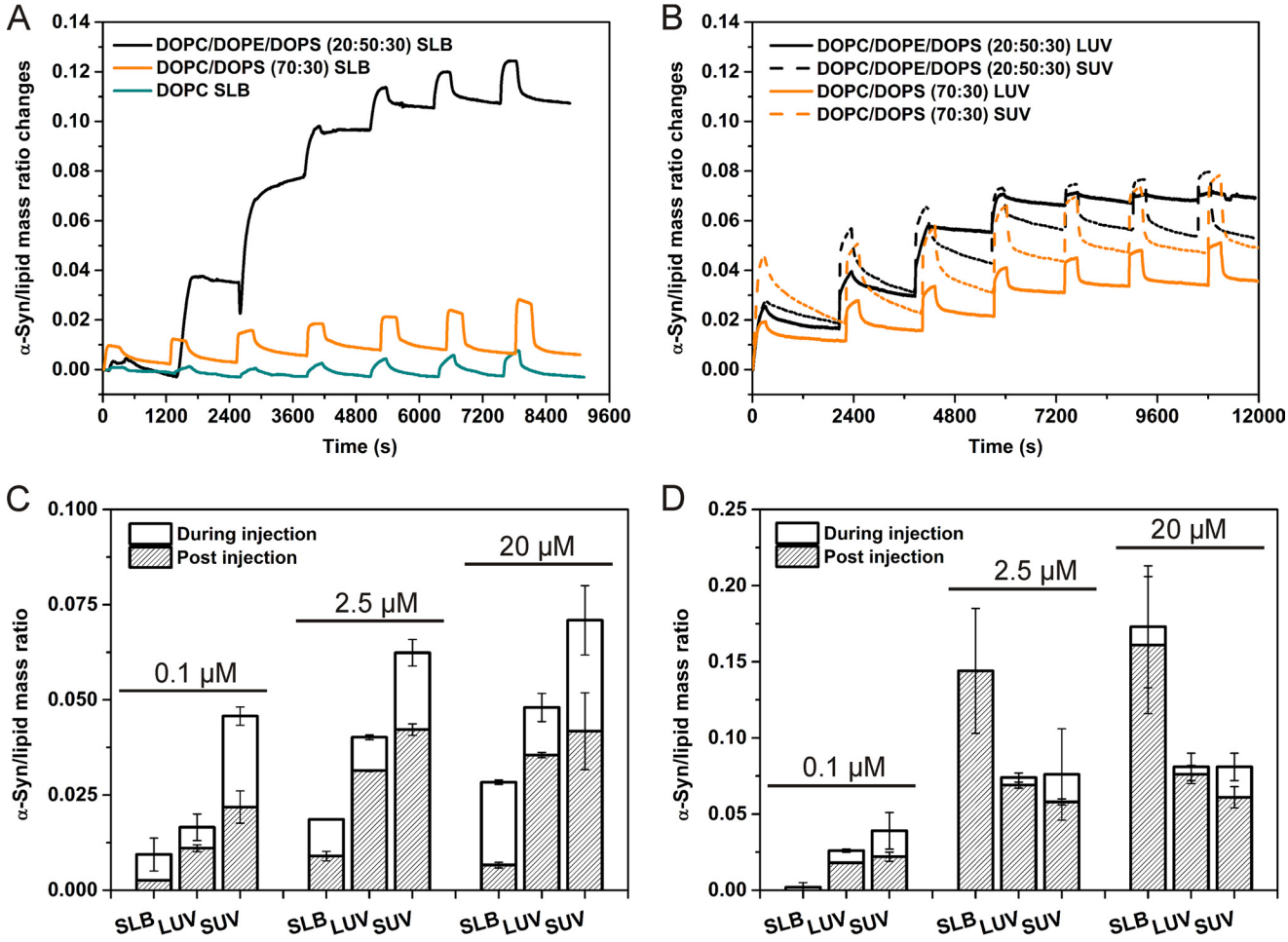

FIGURE 3. **Comparison between different bilayer structures.** Change in α-Syn/lipid mass ratios for consecutive injections of 0.1, 0.5, 1, 2.5, 5, 10, and 20 μM α-Syn in TBS, pH 7.4. *A*, DOPC/DOPE/DOPS (20:50:30) SLB (*black*), DOPC/DOPS (70:30) SLB (*orange*), and DOPC SLB (*cyan*). *B*, DOPC/DOPE/DOPS (20:50:30) LUV (*black line*) and SUV (*black dash*) and DOPC/DOPS (70:30) LUV (*orange line*) and SUV (*orange dash*). Shown is the α-Syn/lipid mass ratio during and after injection at 0.1, 2.5, and 20 μM with DOPC/DOPS (70:30) composition (*C*) and DOPC/DOPE/DOPS (20:50:30) composition (*D*). Protein injections were performed for 5 min, followed by rinsing time with TBS for at least 10 min. Protein/lipid mass ratio values were calculated using the mass values of the corresponding SLBs prior to protein injection together with the additional mass gain after protein injection. The mass changes were determined using the d*n*/d*c* values for proteins and lipids of 0.182 and 0.135 ml/g, respectively (36). The values are the mean of three determinations ± S.D. (*error bars*).

and significant decrease of birefringence (of up to 30% of the initial value). The observed molar ratio is within the same range as that observed for α-Syn (115 ± 50 lipids/protein molecule; Table 2), whereas a significant decrease in the lipid order is measured throughout the interaction. This result is in good agreement with previous observations made for the transmembrane insertion of melittin, which leads to torroidal pore formation and a high disruption of bilayer order (45).

α-Syn Binding to Different Phospholipid Environments

In addition to lipid composition, the effect of bilayer structure on the interaction of α-Syn was compared between planar lipid bilayers and tethered small and large vesicles. Successive injections of increasing concentrations of α-Syn were performed during 5 min on DOPC, DOPC/DOPS (70:30), and DOPC/DOPE/DOPS (20:50:30) planar bilayers, LUVs, and SUVs, followed by rinsing time with TBS for at least 10 min (Fig. 3, *A* and *B*). The changes in protein/lipid mass ratio were monitored during the injection of α-Syn and while rinsing with buffer. The protein/lipid mass ratios at selected concentrations were also compared between SLB, LUV, and SUV structures for DOPC/DOPS and DOPC/DOPE/DOPS, Fig. 3, *C* and *D*, respectively. Only a low level of binding to DOPC SLB (Fig. 3*A*), SUV, or LUV was detected (data not shown). By contrast, DOPC/DOPS (70:30) composition generated a significant binding increase for the different membrane environments, with the highest binding on SUVs (Fig. 3*C*). This binding is partially reversible upon rinsing with buffer. At 20 μM, the binding on SUV reaches a maximum mass ratio of 0.07 ± 0.01 during injection and 0.04 ± 0.01 post-injection. The lipid/protein molar ratio calculated at saturation is ~250.

The presence of DOPE in the SLBs made a dramatic difference. Indeed, the binding of α-Syn was observed to be significantly higher, with a very low degree of reversibility on planar bilayers compared with vesicles. Interestingly, the binding of α-Syn for the DOPC/DOPS mixture shows a trend of SLB < LUV < SUV, whereas for DOPC/DOPE/DOPS, apart from the lowest concentrations, the binding of α-Syn has a different trend of SUV ~ LUV < SLB (Fig. 3, *C* and *D*). The binding of α-Syn to DOPC/DOPE/DOPS SLB shows no reversibility until it reaches saturation following protein incubation. The highest binding of α-Syn is observed for the DOPC/DOPE/DOPS SLB,

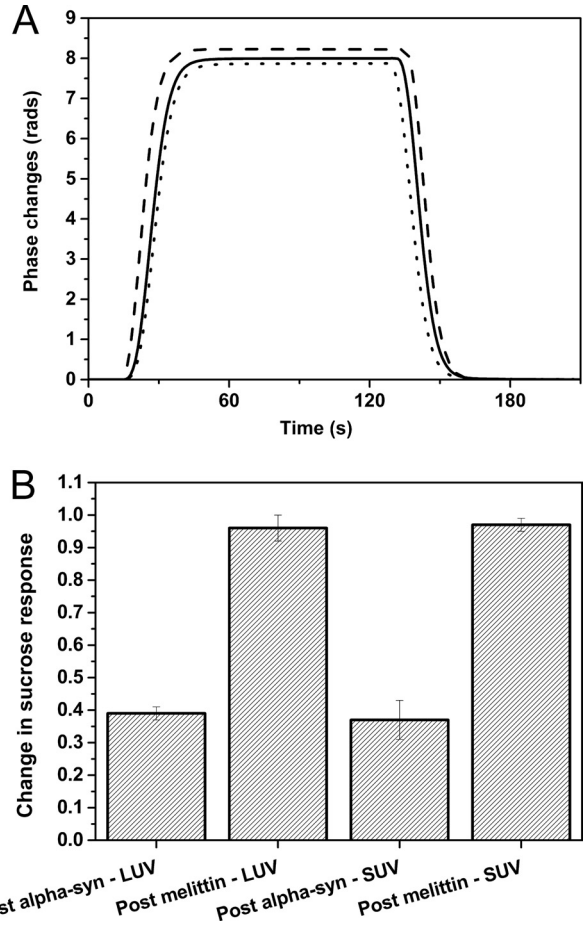

FIGURE 4. **Effect on membrane integrity of the binding of α-Syn and melittin.** *A*, sucrose response prior to vesicle attachment (*dashed line*), after vesicle attachment (*dotted line*), and after α-Syn injections (*solid line*). *B*, change in sucrose response after protein injections on DOPC/DOPE/DOPS (20:50:30) LUV and SUV. The sucrose response corresponds to the measured phase change due to a change in bulk refractive index during the injection of 0.1 M sucrose in TBS. The values are the mean of three determinations ± S.D. (*error bars*).

with a maximum protein/lipid mass ratio of 0.17 ± 0.04 during α-Syn incubation at 20 μM, corresponding to a lipid/protein molar ratio of ~105. The decrease of mass per unit area observed during the first stage of protein binding at 1 μM (Fig. 3*A*) suggests a lipid bilayer rearrangement that could cause a small underestimation of the protein/lipid mass ratio. However, irrespective of this effect, the molar ratio value is within the range of the stoichiometry described for a maximal α-helix folding to DOPC/DOPG (1:1) vesicles (46). It is worth noting that at low α-Syn concentrations, SUVs were observed to induce the highest binding during incubation that rapidly saturated to a mass ratio value of 0.076 ± 0.003, equivalent to DOPC/DOPS (70:30) SUVs (Fig. 3, *B* and *D*). Generally α-Syn binding to SUVs also showed the highest degree of reversibility.

Overall, by comparing all membrane environments, we can describe the following general trend in α-Syn binding: PE SLB ≫ PE LUV ~ PE SUV ~ no PE SUV > no PE LUV > no PE SLB.

Effect of α-Syn on Vesicle Permeability

To gain further insights into the effect of α-Syn binding on vesicles, sucrose injections were performed after protein binding to detect membrane permeabilization (Fig. 4) (42). The sucrose responses following the injections of increasing concentrations of α-Syn and melittin at 2.5 μM were compared with the responses with intact vesicles composed of DOPC/DOPE/DOPS (20:50:30) (Fig. 4*A*). The presence of intact vesicles on the surface reduces the observed bulk refractive index phase response from the sucrose injection due to the excluded volume of the vesicles. A maximum response change, similar to that prior to vesicle attachment, indicates a total loss of vesicle integrity, and the formation of even one pore is sufficient to completely fill a vesicle with sucrose (42). As expected, this effect was observed following melittin injections on LUVs and SUVs (Fig. 4*B*), but α-Syn induces less than 40% of the sucrose response changes with vesicles. This apparent partial loss of

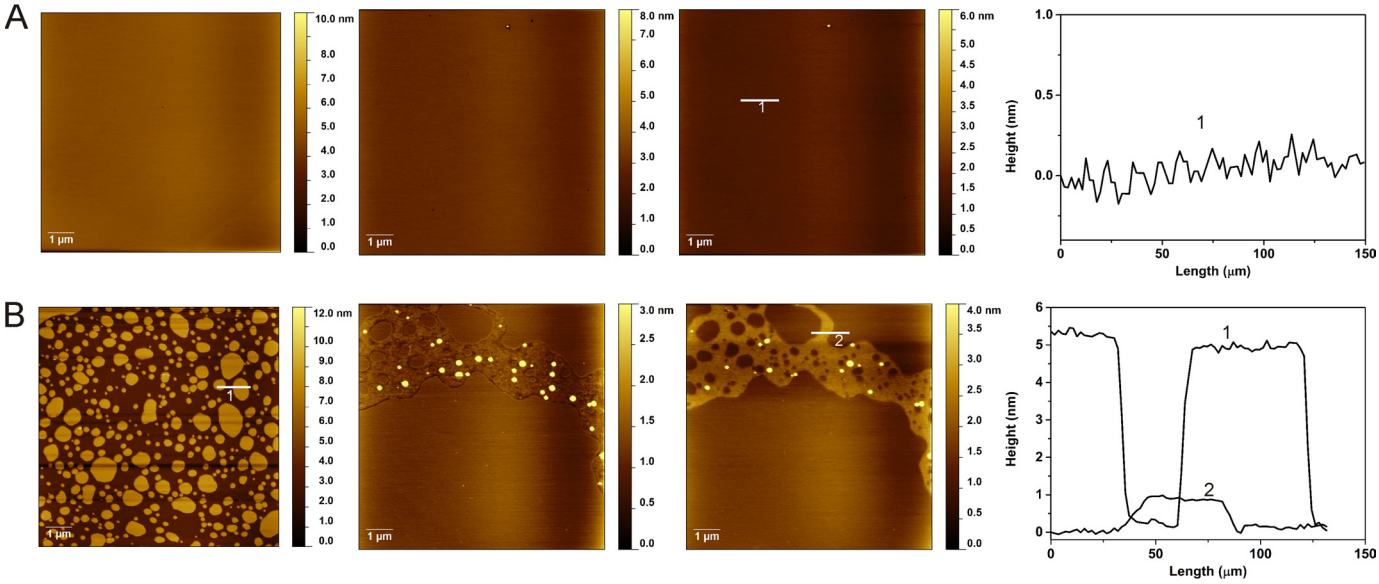

FIGURE 5. **Morphological changes of DOPC/DOPE/DOPS (20:50:30) SLBs.** AFM images of a defect-free DOPC/DOPE/DOPS (20:50:30) SLB incubated with 1 μM α-Syn (*A*) and an incomplete DOPC/DOPE/DOPS (20:50:30) SLB incubated with 1 μM α-Syn (*B*). The *first column* shows images prior to incubation, the *second column* shows images following 20 min of incubation, the *third column* shows images after 60 min of incubation, and the *fourth column* corresponds to the height profiles along the *white lines* indicated by numbers.

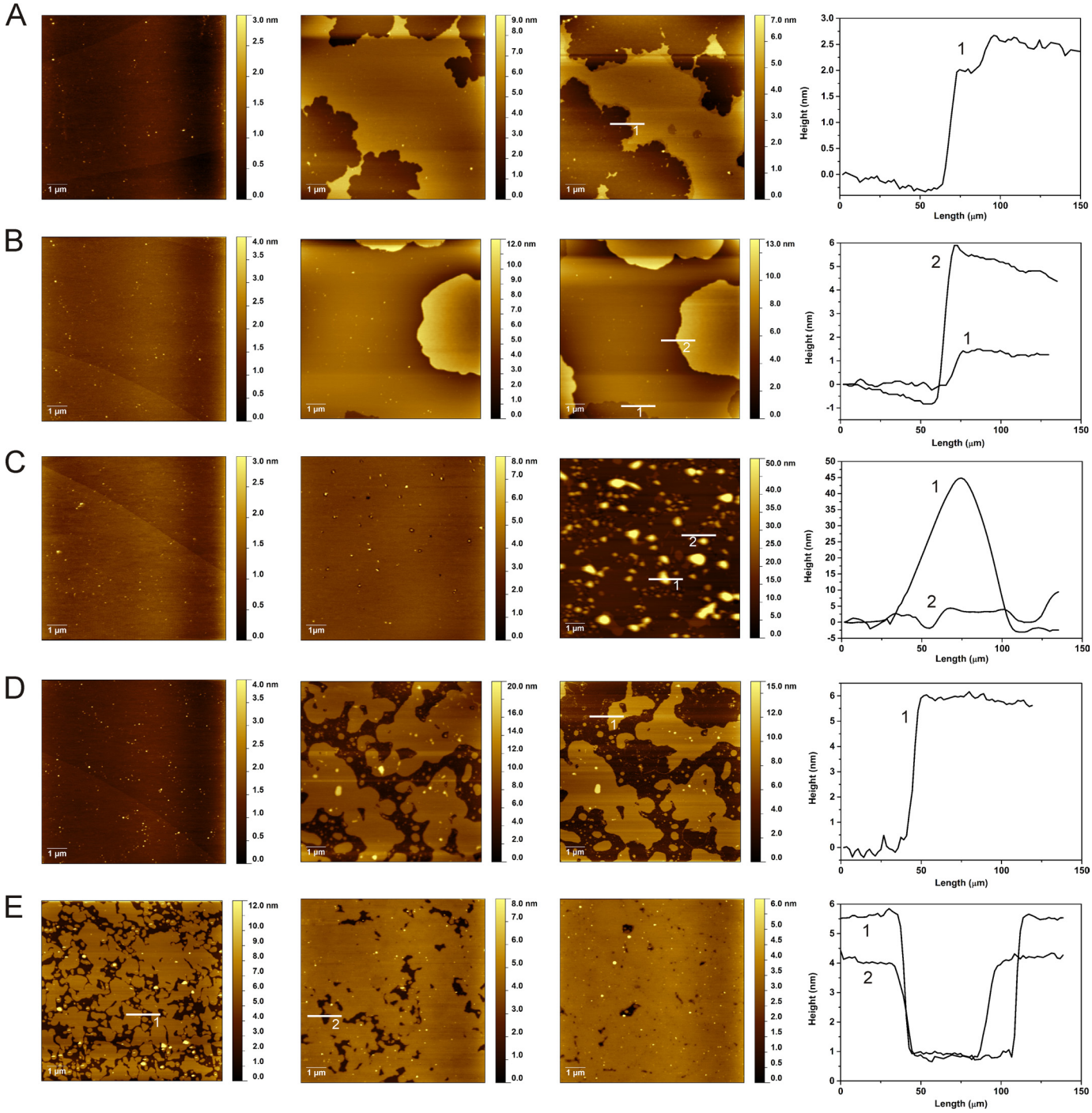

FIGURE 6. **Morphological changes of brain total lipid extract SLBs.** AFM images of BTLE SLBs incubated with α-Syn at 1 μM (*A*) and 25 μM (*B*) and with melittin at 1 μM (*C*) and 25 μM (*D*) and 10% ethanol (*E*). The *first column* shows images prior to incubation, the *second column* shows images following 20 min of incubation, the *third column* shows images after 60 min of incubation, and the *fourth column* corresponds to the height profiles along the *white lines* indicated by numbers.

vesicle integrity is very significantly lower than the permeabilization effect due to pore formation observed with melittin and at most would represent the permeabilization of a subset of the immobilized vesicles.

Effect of α-Syn on Planar Bilayer Structure

AFM studies were performed to investigate the effect of α-Syn binding on the structure of lipid bilayers composed of DOPC/DOPE/DOPS (20:50:30). After formation of a defect-free supported lipid bilayer, as shown in Fig. 5*A* (*first column*), α-Syn was introduced, and the morphological changes in the lipid bilayers were followed with time. No noticeable change in the bilayer structure was observed with the DOPC/DOPE/DOPS (20:50:30) composition following incubation with α-Syn at 1 μM (Fig. 5*A*). Considering the lag time between the addition of the protein to the SLB and the first image acquisition (at least 10 min), an incomplete SLB showing a height difference of ~5 nm was co-incubated with α-Syn at 1 μM (Fig. 5*B*). The first

images reveal significant structural changes, with a lateral spreading of lipids leading to the formation of a defect-free lipid bilayer with domains having different morphologies. The step height measured between an elevated rough domain and a smooth domain was ~1 nm. One can notice the presence of protrusions having heights ranging from 5 to 20 nm within the rough domain. It is interesting that, apart from the slow disappearance of these protrusions, no further morphological changes were observed.

In order to use a more physiologically relevant composition of lipids, a BTLE was selected. Following incubation of α-Syn at 1 μM with a defect-free SLB made of this extract, a gradual formation and expansion of lipid bilayer defects was observed (Fig. 6*A*). The progression of defects appears to develop from a small number of nucleation areas. The depth of these defects is estimated to be 3–3.5 nm (*i.e.* less than the thickness of the bilayer). A second defect can also be observed with a depth of 0.7 nm. These step heights appear to correspond to membrane structural changes and especially to the formation of thinner phases. At a higher concentration with BTLE SLBs, as seen in Fig. 6*B*, the expansion of these reduced step heights is also observed, but the depth is about 1.5 nm. The most significant rearrangement that can be visualized is the formation of higher steps of about 6 nm that can be related to expansion of lipids out of the membrane plane.

Previous AFM imaging studies have revealed the disruption by α-Syn of highly negative supported lipid bilayers made of 1,2-dipalmitoyl-*sn*-glycero-3-phosphate/1,2-dipalmitoyl-*sn*-glycero-3-phosphocholine (1:1) and 1-palmitoyl-2-oleoyl-*sn*-glycero-3-phospho-L-serine/1-palmitoyl-2-oleoyl-*sn*-glycero-3-phosphocholine (1:1) (23, 30). The defects observed were mainly described as bilayer holes, but no binding mode has been proposed to explain their formation. Therefore, melittin known to form pores was incubated with lipid bilayers made of BTLE at 1 μM in order to compare with the effects induced by α-Syn (Fig. 6*C*). In the first 20 min, we observed the formation of small defects, which slowly progressed toward more significant rearrangements. These effects can be described as lower steps with a depth of about 5 nm and higher protrusions of about 45 nm in height. Increasing the concentration of melittin to 25 μM induces formation of holes with a depth corresponding to the bilayer thickness of about 6 nm (Fig. 6*D*). Melittin is known to interact with lipid membranes through a two-state mechanism that depends on the bound peptide/lipid ratio (45). Below a certain threshold ratio, the peptide binds in a helical conformation with its axis oriented parallel to the membrane, similar to the conformation proposed for α-Syn. In this conformation, the peptide causes membrane thinning and formation of tubules, as reported previously (47). Above this threshold ratio, the peptide adopts an orientation perpendicular to the plane of the membrane, and transmembrane pores are formed. This mechanism is in good agreement with the observations made in the present study.

In order to gain more insight into the structural rearrangements of the bilayers induced by α-Syn, an incomplete lipid bilayer made of BTLE was incubated with 10% ethanol, which is known to induce thinning of the lipid membranes. As observed in Fig. 6*E*, the initial bilayer thickness of about 5 nm decreases to 3–3.5 nm, values similar to the defect depth observed during α-Syn incubation. Moreover, this thinning is accompanied by a reduction in the number and surface area of bilayer defects related to a lateral expansion of lipids.

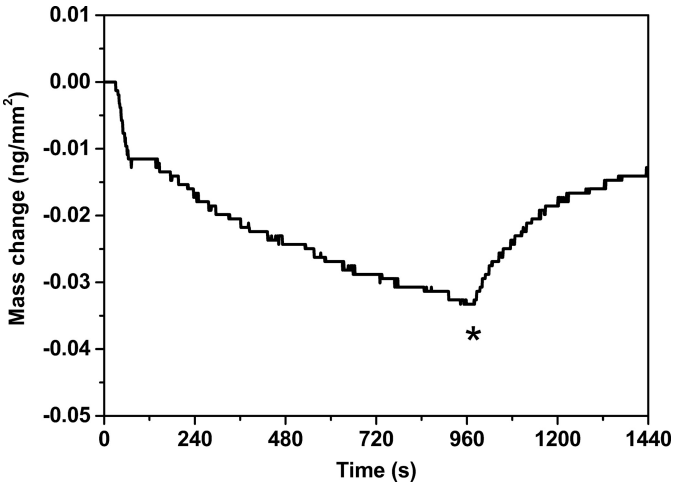

FIGURE 7. **DPI study with brain total lipid extract SLB.** Mass change upon incubation of brain total lipid extract SLB with 2.5 μM α-Syn. *, the protein solution has been replaced by the protein-free buffer solution.

Finally, in order to understand further the rearrangements observed with BTLE, α-Syn binding to SLB made of this extract was monitored using DPI. α-Syn was incubated at 2.5 μM for 15 min with the SLB, and as seen in Fig. 7, a slow and continuous decrease of mass per unit area was observed during injection that can be attributed to a thinning and lateral expansion of the lipid bilayer. Upon rinsing of the protein from the SLB, a slow mass increase per unit area was observed, confirming that the process induced by α-Syn upon binding is reversed and not attributable to lipid removal.

DISCUSSION

In the past few years, α-Syn has been a subject of extremely high interest because of its link with Parkinson disease (1). Its exact physiological function remains to be established, but there is substantial evidence for its involvement in vesicle trafficking (3). Although previous studies have described the effects of membranes on the binding, structure, and aggregation propensity of α-Syn, few have focused on the effects of binding on the membrane structure and how any structural changes are correlated with the mode of interaction. Lipid membranes are dynamic structures, and bilayer remodeling can be a consequence of the interaction between lipid components and proteins (48). It is now well established that α-Syn is unfolded in solution and undergoes a conformational change into a highly helical structure upon interaction with membranes; this has been shown, in particular, with DOPC/DOPE/DOPS (20:50:30) SUVs, for which the 100 N-terminal residues of α-Syn adopt an α-helical conformation, whereas the 40 C-terminal residues remain disordered (10). This structural change has been further confirmed upon interaction with DOPC/DOPE/DOPS (20:50:30) LUVs in the present study.

Our data demonstrate that, with the same lipid/protein molar ratio, α-Syn affects the degree of ordering of membrane to a significantly lesser extent than observed with melittin. This

Effects of α-Synuclein Insertion on Membrane Structure and Dynamics

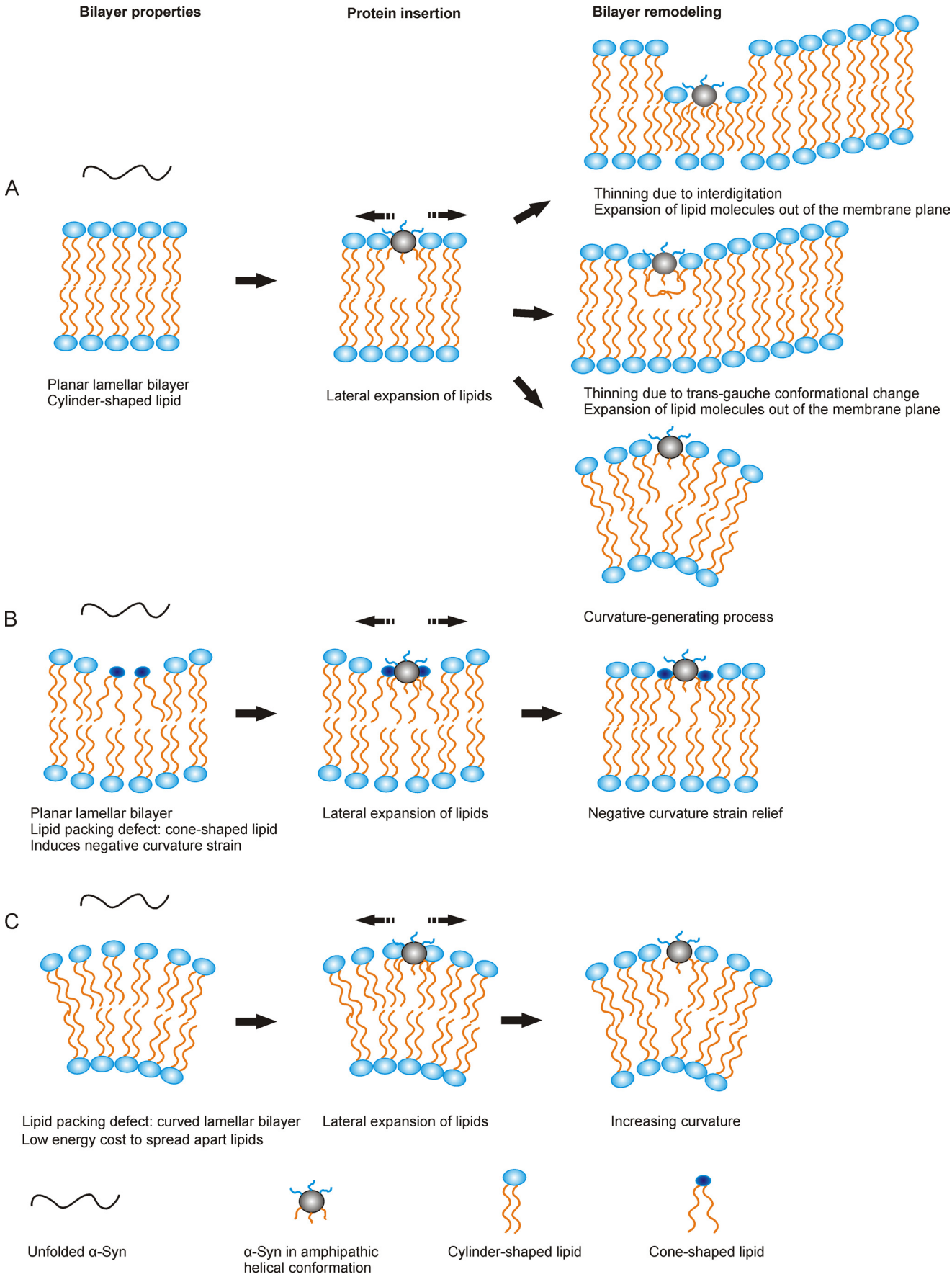

result suggests that α-Syn interacts with membranes in the region of the phospholipid headgroups, in good agreement with previous results showing that the protein binds to the surface of the lipid bilayer in an α-helical conformation with its axis parallel to the surface (20). Structural rearrangement into an α-helical structure upon interaction with lipid membranes is a well known phenomenon for peptides and proteins with ALPS motifs (11). Although both ALPS motifs and α-Syn are described as curvature-sensing, their amphipathic characteristics are different, because ALPS motifs use bulky hydrophobic residues as an interaction force, whereas as observed in this study, α-Syn uses electrostatic interactions (11, 13, 17). Although α-Syn has a different set of residue types from ALPS motif, it appears to sense lipid packing defects that influence the binding affinity. Curvature of the binding interface and cone-shaped lipids induce lipid packing defects because of the mismatch between the curvature of the bilayer and the shape of the lipid (11, 49, 50). The binding enhancement due to curvature can be explained by the reduced degree of lipid headgroup packing because a less compact environment between headgroups promotes insertion of the hydrophobic residues. This reduces the energy cost for lipid spreading upon binding, and less membrane rearrangement is necessary to accommodate protein insertion. The presence of conical lipids in planar bilayers has been shown to impose a stress over the lipid membrane, leading to the formation of defects or imperfections in packing similar to positive curvature (50).

The present data suggest that for lipid bilayers with cone-shaped lipids, an additional less reversible mechanism enhancing binding also plays a significant part. Indeed, the variation in affinity in the presence of PE is opposite to that expected from a curvature sensor model, with stronger binding on SLBs compared with vesicles. This tendency is not dominant at low concentrations of protein (where the binding is not close to saturation). However, at higher concentrations, for lipid bilayers containing PE, more protein is bound irreversibly to the more planar bilayers. The presence of PE within the planar lamellar bilayer appears to provide more binding sites for protein insertion, and the binding appears less reversible because the lipids have to undergo more rearrangement to accommodate α-Syn. Moreover, the decrease of mass per surface area, observed at the initial stage of binding, matches well with a model in which the protein induces a significant lateral expansion of the lipids upon insertion in order to bridge the spaces between headgroups and relieve the negative curvature strain induced by the high PE content in the lamellar phase (43).

The results obtained in this study demonstrate that the binding affinity correlates with the ability of the membranes to accommodate protein insertion upon binding by means of curvature or the presence of cone-shaped lipids as protein insertion induces a lateral expansion of lipids; this finding is closely linked to membrane remodeling. Several mechanisms can be responsible for a membrane thinning process leading to different step heights, from hydrocarbon chain trans-gauche conformational changes (51) to the formation of an interdigitated phase (52, 53). Interdigitation of molecules in membranes is a process that has been widely studied in the presence of ethanol and arises from an increase in the lateral area between lipid headgroups by the insertion of ethanol molecules (54, 55). The void created at the acyl chain level results in a rearrangement in which the acyl chains of one lipid monolayer interpenetrate the opposite layer (52). We have shown that an interdigitation process can occur with BTLE in the presence of ethanol because a clear lateral expansion of lipids associated with a decrease of the thickness of the bilayers in the same range as the depth of the defects induced by α-Syn has been observed. In the presence of a high α-Syn concentration, bilayer thinning and lipid expansion out of the membrane plane are also observed. This latter effect can also be related to the lateral expansion of the lipid molecules that induces membrane thinning and, with further insertion of protein into the membrane, causes lipid expansion out of the membrane plane of the bilayer or, as previously reported, formation of positive curvature to relieve excess surface pressure (56, 57). A close relationship between amphipathic helix insertion and membrane deformation has been established (57), and α-Syn has been reported to induce positive curvature of the membrane and the formation of tubular structures (26, 58, 59). Recently, these remodeling processes caused by α-Syn binding have been proposed to induce the formation of lipoprotein nanoparticles (60).

The membrane thinning process has been suggested to occur with α-Syn (58, 61, 62) and with amphipathic peptides or proteins (51, 63). However, in the case of α-Syn, no binding mode has been proposed to explain these processes. These membrane remodeling processes are closely linked to the affinity of the amphipathic helices for lipid packing defects and to the ability of the lipid bilayer to rearrange upon protein insertion to accommodate lateral expansion of lipids. Interestingly, some significant remodeling of DOPC/DOPE/DOPS (20:50:30) SUVs in the presence of very high concentrations of α-Syn has been observed and described as the formation of multilamellar and tubular structures (10). No such structures or remodeling processes of supported lipid bilayers, observed with BTLE, were observed with complete DOPC/DOPE/DOPS (20:50:30) bilayers. However, rapid and extensive bilayer spreading, along with formation of domains, was observed for surfaces covered with DOPC/DOPE/DOPS (20:50:30) bilayer patches. These rearrangements, which are similar to those observed with ethanol, correspond to a lateral expansion of lipids changing their packing and leading to the formation of domains. The lack of evident remodeling of complete bilayers can be attributed to the rapidity of a limited remodeling process (just a lateral expansion of lipids) for DOPC/DOPE/DOPS (20:50:30), which can be faster than the lag time between the addition of the protein to the SLB

FIGURE 8. **Model of α-Syn binding to membranes and lipid bilayer remodeling processes.** *A*, a planar lamellar bilayer composed of cylinder-shaped lipids. Lateral expansion of the lipids induces a void in the bilayer core that rearranges to minimize the energy. Membrane remodeling processes range from membrane thinning to expansion of lipids out of the membrane plane and a curvature-generating process, as reported previously (28, 59). *B*, a planar lamellar bilayer with a high content of cone-shaped lipids. The lateral expansion of the lipids is enhanced by the relief of the negative curvature strain induced by cone-shaped lipids. Further remodeling can occur, depending on the conditions (10). *C*, a curved lamellar bilayer with loosely packed lipids that reduces the energy cost of lateral expansion. A possible remodeling could be a curvature increase, as reported previously (26).

and the first image acquisition, together with a lack of sufficient protein adsorption to force the more significant bilayer remodeling. This latter case can be related to the fact that these processes occur in particular conditions of lipid composition and lipid/protein ratios.

Another important issue addressed in this work is the effect of α-Syn on the membrane permeability, and no transmembrane insertion of α-Syn or formation of pores has been observed. This conclusion is drawn from comparison of the effects of α-Syn and melittin on planar bilayers as well as on vesicles. Melittin induces a large decrease of birefringence, a total loss of vesicle integrity, and the formation of pores in the supported bilayers. Melittin is known to interact with lipid membranes through a two-state mechanism dependent on the bound peptide/lipid ratio, leading to membrane remodeling or transmembrane pore formation (45, 47). We suggest that a partial loss of membrane integrity upon α-Syn binding, as observed in our sucrose response study, could arise from bilayer deformation, as suggested previously (26). Indeed, curvature stress and change in bilayer thickness can increase the permeability of lipid bilayers due to osmotic stress. These processes could induce a nonspecific permeabilization effect that does not affect the whole population of vesicles, as compared with a pore formation mechanism that would result in a complete permeabilization.

A proposed model for the interaction of α-Syn with lipid bilayers and the ability of membranes to accommodate and remodel upon protein insertion is illustrated in Fig. 8, which is based on results obtained in the present study and also those reported in the literature (10, 26, 28, 59). Lipid membranes are dynamic structures, and, under appropriate conditions of lipid composition and bilayer structure, they enable protein insertion to occur. The binding of α-Syn to lipid bilayers involves insertion at the headgroup region that induces lateral expansion of lipids. This insertion is facilitated and enhanced by lipid packing defects resulting from the presence of cone-shaped lipids or the existence of membrane curvature. To accommodate lateral expansion of lipids, membrane remodeling can then occur, resulting in effects such as membrane thinning and the expansion of lipids out of the membrane plane. Finally, we can relate the proposed binding mode to vesicle trafficking, because structural changes in cellular membranes are the first steps of vesicle budding and fusion, supported by the strong relationship that exists between curvature-sensing proteins and dynamic membrane remodeling (48).

Acknowledgments—We thank Prof. Jian R. Lu for help with dynamic light scattering measurements and Dr. Alexander K. Buell for extremely helpful discussions and advice. We thank Layerlab for providing the DNA coupling kit.

REFERENCES

1. Spillantini, M. G., Schmidt, M. L., Lee, V. M., Trojanowski, J. Q., Jakes, R., and Goedert, M. (1997) α-Synuclein in Lewy bodies. *Nature* **388,** 839–840
2. Chiti, F., and Dobson, C. M. (2006) Protein misfolding, functional amyloid, and human disease. *Annu. Rev. Biochem.* **75,** 333–366
3. Auluck, P. K., Caraveo, G., and Lindquist, S. (2010) α-Synuclein. Membrane interactions and toxicity in Parkinson's disease. *Annu. Rev. Cell Dev. Biol.* **26,** 211–233
4. Fortin, D. L., Troyer, M. D., Nakamura, K., Kubo, S., Anthony, M. D., and Edwards, R. H. (2004) Lipid rafts mediate the synaptic localization of α-synuclein. *J. Neurosci.* **24,** 6715–6723
5. Outeiro, T. F., and Lindquist, S. (2003) Yeast cells provide insight into α-synuclein biology and pathobiology. *Science* **302,** 1772–1775
6. Gitler, A. D., Bevis, B. J., Shorter, J., Strathearn, K. E., Hamamichi, S., Su, L. J., Caldwell, K. A., Caldwell, G. A., Rochet, J. C., McCaffery, J. M., Barlowe, C., and Lindquist, S. (2008) The Parkinson's disease protein α-synuclein disrupts cellular Rab homeostasis. *Proc. Natl. Acad. Sci. U.S.A.* **105,** 145–150
7. Drin, G., and Antonny, B. (2010) Amphipathic helices and membrane curvature. *FEBS Lett.* **584,** 1840–1847
8. Ulmer, T. S., Bax, A., Cole, N. B., and Nussbaum, R. L. (2005) Structure and dynamics of micelle-bound human α-synuclein. *J. Biol. Chem.* **280,** 9595–9603
9. Bodner, C. R., Maltsev, A. S., Dobson, C. M., and Bax, A. (2010) Differential phospholipid binding of α-synuclein variants implicated in Parkinson's disease revealed by solution NMR spectroscopy. *Biochemistry* **49,** 862–871
10. Bodner, C. R., Dobson, C. M., and Bax, A. (2009) Multiple tight phospholipid-binding modes of α-synuclein revealed by solution NMR spectroscopy. *J. Mol. Biol.* **390,** 775–790
11. Antonny, B. (2011) Mechanisms of membrane curvature sensing. *Annu. Rev. Biochem.* **80,** 101–123
12. Drin, G., Casella, J. F., Gautier, R., Boehmer, T., Schwartz, T. U., and Antonny, B. (2007) A general amphipathic α-helical motif for sensing membrane curvature. *Nat. Struct. Mol. Biol.* **14,** 138–146
13. Pranke, I. M., Morello, V., Bigay, J., Gibson, K., Verbavatz, J. M., Antonny, B., and Jackson, C. L. (2011) α-Synuclein and ALPS motifs are membrane curvature sensors whose contrasting chemistry mediates selective vesicle binding. *J. Cell Biol.* **194,** 89–103
14. Pfefferkorn, C. M., Jiang, Z., and Lee, J. C. (2012) Biophysics of α-synuclein membrane interactions. *Biochim. Biophys. Acta* **1818,** 162–171
15. Middleton, E. R., and Rhoades, E. (2010) Effects of curvature and composition on α-synuclein binding to lipid vesicles. *Biophys. J.* **99,** 2279–2288
16. Nuscher, B., Kamp, F., Mehnert, T., Odoy, S., Haass, C., Kahle, P. J., and Beyer, K. (2004) α-Synuclein has a high affinity for packing defects in a bilayer membrane. A thermodynamics study. *J. Biol. Chem.* **279,** 21966–21975
17. Davidson, W. S., Jonas, A., Clayton, D. F., and George, J. M. (1998) Stabilization of α-synuclein secondary structure upon binding to synthetic membranes. *J. Biol. Chem.* **273,** 9443–9449
18. Martinez, Z., Zhu, M., Han, S., and Fink, A. L. (2007) GM1 specifically interacts with α-synuclein and inhibits fibrillation. *Biochemistry* **46,** 1868–1877
19. Kubo, S., Nemani, V. M., Chalkley, R. J., Anthony, M. D., Hattori, N., Mizuno, Y., Edwards, R. H., and Fortin, D. L. (2005) A combinatorial code for the interaction of α-synuclein with membranes. *J. Biol. Chem.* **280,** 31664–31672
20. Jao, C. C., Hegde, B. G., Chen, J., Haworth, I. S., and Langen, R. (2008) Structure of membrane-bound α-synuclein from site-directed spin labeling and computational refinement. *Proc. Natl. Acad. Sci. U.S.A.* **105,** 19666–19671
21. Georgieva, E. R., Ramlall, T. F., Borbat, P. P., Freed, J. H., and Eliezer, D. (2010) The lipid-binding domain of wild type and mutant α-synuclein. Compactness and interconversion between the broken and extended helix forms. *J. Biol. Chem.* **285,** 28261–28274
22. Kim, H. Y., Cho, M. K., Kumar, A., Maier, E., Siebenhaar, C., Becker, S., Fernandez, C. O., Lashuel, H. A., Benz, R., Lange, A., and Zweckstetter, M. (2009) Structural properties of pore-forming oligomers of α-synuclein. *J. Am. Chem. Soc.* **131,** 17482–17489
23. Zhu, M., Li, J., and Fink, A. L. (2003) The association of α-synuclein with membranes affects bilayer structure, stability, and fibril formation. *J. Biol. Chem.* **278,** 40186–40197
24. van Rooijen, B. D., Claessens, M. M., and Subramaniam, V. (2010) Membrane permeabilization by oligomeric α-synuclein. In search of the mech-

anism. *PloS One* **5,** e14292
25. Zakharov, S. D., Hulleman, J. D., Dutseva, E. A., Antonenko, Y. N., Rochet, J. C., and Cramer, W. A. (2007) Helical α-synuclein forms highly conductive ion channels. *Biochemistry* **46,** 14369–14379
26. Varkey, J., Isas, J. M., Mizuno, N., Jensen, M. B., Bhatia, V. K., Jao, C. C., Petrlova, J., Voss, J. C., Stamou, D. G., Steven, A. C., and Langen, R. (2010) Membrane curvature induction and tubulation are common features of synucleins and apolipoproteins. *J. Biol. Chem.* **285,** 32486–32493
27. Pandey, A. P., Haque, F., Rochet, J. C., and Hovis, J. S. (2011) α-Synuclein-induced tubule formation in lipid bilayers. *J. Phys. Chem. B* **115,** 5886–5893
28. Mizuno, N., Varkey, J., Kegulian, N. C., Hegde, B. G., Cheng, N., Langen, R., and Steven, A. C. (2012) Remodeling of lipid vesicles into cylindrical micelles by α-synuclein in an extended α-helical conformation. *J. Biol. Chem.* **287,** 29301–29311
29. Zhu, M., and Fink, A. L. (2003) Lipid binding inhibits α-synuclein fibril formation. *J. Biol. Chem.* **278,** 16873–16877
30. Jo, E., McLaurin, J., Yip, C. M., St George-Hyslop, P., and Fraser, P. E. (2000) α-Synuclein membrane interactions and lipid specificity. *J. Biol. Chem.* **275,** 34328–34334
31. Lee, H. J., Choi, C., and Lee, S. J. (2002) Membrane-bound α-synuclein has a high aggregation propensity and the ability to seed the aggregation of the cytosolic form. *J. Biol. Chem.* **277,** 671–678
32. Cole, N. B., Murphy, D. D., Grider, T., Rueter, S., Brasaemle, D., and Nussbaum, R. L. (2002) Lipid droplet binding and oligomerization properties of the Parkinson's disease protein α-synuclein. *J. Biol. Chem.* **277,** 6344–6352
33. Comellas, G., Lemkau, L. R., Zhou, D. H., George, J. M., and Rienstra, C. M. (2012) Structural intermediates during α-synuclein fibrillogenesis on phospholipid vesicles. *J. Am. Chem. Soc.* **134,** 5090–5099
34. Freeman, N. J., Peel, L. L., Swann, M. J., Cross, G. H., Reeves, A., Brand, S., and Lu, J. R. (2004) Real time, high resolution studies of protein adsorption and structure at the solid-liquid interface using dual polarization interferometry. *J. Phys.-Condes. Matter* **16,** S2493–S2496
35. Xu, K., Ouberai, M. M., and Welland, M. E. (2013) A comprehensive study of lysozyme adsorption using dual polarization interferometry and quartz crystal microbalance with dissipation. *Biomaterials* **34,** 1461–1470
36. Mashaghi, A., Swann, M., Popplewell, J., Textor, M., and Reimhult, E. (2008) Optical anisotropy of supported lipid structures probed by waveguide spectroscopy and its application to study of supported lipid bilayer formation kinetics. *Anal. Chem.* **80,** 3666–3676
37. Lee, T. H., Hall, K. N., Swann, M. J., Popplewell, J. F., Unabia, S., Park, Y., Hahm, K. S., and Aguilar, M. I. (2010) The membrane insertion of helical antimicrobial peptides from the N-terminus of *Helicobacter pylori* ribosomal protein L1. *Biochim. Biophys. Acta* **1798,** 544–557
38. Nielsen, S. B., and Otzen, D. E. (2010) Impact of the antimicrobial peptide Novicidin on membrane structure and integrity. *J. Colloid Interface Sci.* **345,** 248–256
39. Singh, S., Kasetty, G., Schmidtchen, A., and Malmsten, M. (2012) Membrane and lipopolysaccharide interactions of C-terminal peptides from S1 peptidases. *Biochim. Biophys. Acta* **1818,** 2244–2251
40. Hoyer, W., Antony, T., Cherny, D., Heim, G., Jovin, T. M., and Subramaniam, V. (2002) Dependence of α-synuclein aggregate morphology on solution conditions. *J. Mol. Biol.* **322,** 383–393
41. Coan, K. E., Swann, M. J., and Ottl, J. (2012) Measurement and differentiation of ligand-induced calmodulin conformations by dual polarization interferometry. *Anal. Chem.* **84,** 1586–1591
42. Brändén, M., Dahlin, S., and Höök, F. (2008) Label-free measurements of molecular transport across liposome membranes using evanescent-wave sensing. *ChemPhysChem* **9,** 2480–2485
43. Hauser, H., Pascher, I., Pearson, R. H., and Sundell, S. (1981) Preferred conformation and molecular packing of phosphatidylethanolamine and phosphatidylcholine. *Biochim. Biophys. Acta* **650,** 21–51
44. Granéli, A., Edvardsson, M., and Höök, F. (2004) DNA-based formation of a supported, three-dimensional lipid vesicle matrix probed by QCM-D and SPR. *ChemPhysChem* **5,** 729–733
45. Huang, H. W. (2006) Molecular mechanism of antimicrobial peptides. The origin of cooperativity. *Biochim. Biophys. Acta* **1758,** 1292–1302
46. Shvadchak, V. V., Yushchenko, D. A., Pievo, R., and Jovin, T. M. (2011) The mode of α-synuclein binding to membranes depends on lipid composition and lipid to protein ratio. *FEBS Lett.* **585,** 3513–3519
47. Machán, R., Miszta, A., Hermens, W., and Hof, M. (2010) Real-time monitoring of melittin-induced pore and tubule formation from supported lipid bilayers and its physiological relevance. *Chem. Phys. Lipids* **163,** 200–206
48. McMahon, H. T., and Gallop, J. L. (2005) Membrane curvature and mechanisms of dynamic cell membrane remodelling. *Nature* **438,** 590–596
49. Antonny, B., Huber, I., Paris, S., Chabre, M., and Cassel, D. (1997) Activation of ADP-ribosylation factor 1 GTPase-activating protein by phosphatidylcholine-derived diacylglycerols. *J. Biol. Chem.* **272,** 30848–30851
50. Vamparys, L., Gautier, R., Vanni, S., Bennett, W. F., Tieleman, D. P., Antonny, B., Etchebest, C., and Fuchs, P. F. (2013) Conical lipids in flat bilayers induce packing defects similar to that induced by positive curvature. *Biophys. J.* **104,** 585–593
51. Heller, W. T., Waring, A. J., Lehrer, R. I., Harroun, T. A., Weiss, T. M., Yang, L., and Huang, H. W. (2000) Membrane thinning effect of the β-sheet antimicrobial protegrin. *Biochemistry* **39,** 139–145
52. Slater, J. L., and Huang, C. H. (1988) Interdigitated bilayer membranes. *Prog. Lipid Res.* **27,** 325–359
53. Canale, C., Torrassa, S., Rispoli, P., Relini, A., Rolandi, R., Bucciantini, M., Stefani, M., and Gliozzi, A. (2006) Natively folded HypF-N and its early amyloid aggregates interact with phospholipid monolayers and destabilize supported phospholipid bilayers. *Biophys. J.* **91,** 4575–4588
54. Kranenburg, M., Vlaar, M., and Smit, B. (2004) Simulating induced interdigitation in membranes. *Biophys. J.* **87,** 1596–1605
55. Ly, H. V., and Longo, M. L. (2004) The influence of short-chain alcohols on interfacial tension, mechanical properties, area/molecule, and permeability of fluid lipid bilayers. *Biophys. J.* **87,** 1013–1033
56. Domanov, Y. A., and Kinnunen, P. K. (2006) Antimicrobial peptides temporins B and L induce formation of tubular lipid protrusions from supported phospholipid bilayers. *Biophys. J.* **91,** 4427–4439
57. Gallop, J. L., and McMahon, H. T. (2005) BAR domains and membrane curvature. Bringing your curves to the BAR. *Biochem. Soc. Symp.* 223–231
58. Braun, A. R., Sevcsik, E., Chin, P., Rhoades, E., Tristram-Nagle, S., and Sachs, J. N. (2012) α-Synuclein induces both positive mean curvature and negative Gaussian curvature in membranes. *J. Am. Chem. Soc.* **134,** 2613–2620
59. Westphal, C. H., and Chandra, S. S. (2013) Monomeric synucleins generate membrane curvature. *J. Biol. Chem.* **288,** 1829–1840
60. Varkey, J., Mizuno, N., Hegde, B. G., Cheng, N., Steven, A. C., and Langen, R. (2013) α-Synuclein oligomers with broken helical conformation form lipoprotein nanoparticles. *J. Biol. Chem.* **288,** 17620–17630
61. Pfefferkorn, C. M., Heinrich, F., Sodt, A. J., Maltsev, A. S., Pastor, R. W., and Lee, J. C. (2012) Depth of α-synuclein in a bilayer determined by fluorescence, neutron reflectometry, and computation. *Biophys. J.* **102,** 613–621
62. Reynolds, N. P., Soragni, A., Rabe, M., Verdes, D., Liverani, E., Handschin, S., Riek, R., and Seeger, S. (2011) Mechanism of membrane interaction and disruption by α-synuclein. *J. Am. Chem. Soc.* **133,** 19366–19375
63. Mecke, A., Lee, D. K., Ramamoorthy, A., Orr, B. G., and Banaszak Holl, M. M. (2005) Membrane thinning due to antimicrobial peptide binding. An atomic force microscopy study of MSI-78 in lipid bilayers. *Biophys. J.* **89,** 4043–4050